Hindawi
Advances in Materials Science and Engineering
Volume 2021, Article ID 6953756, 9 pages
https://doi.org/10.1155/2021/6953756

Research Article

Effect of Welding Wires Containing ZrB_2 Particles on Microstructure and Mechanical Properties of Spray-Formed 7055 Aluminum Alloy TIG Welded Joints

Ting Huang,[1,2] **Junhua Xu**,[1] **Lihua Yu**,[1] **Yunxuan Hu**,[1] **Yun Cheng**,[1] **and Hao Zhang**[1]

[1]*School of Materials Science and Engineering, Jiangsu University of Science and Technology, Zhenjiang 212003, China*
[2]*Metal Material Engineering, Jiangsu University Jingjiang College, Zhenjiang 212028, China*

Correspondence should be addressed to Junhua Xu; jhxu@just.edu.cn

Received 9 April 2021; Revised 4 June 2021; Accepted 7 July 2021; Published 20 July 2021

Academic Editor: Yee-wen Yen

In this paper, a series of welding wires with ZrB_2 particles were developed by the in situ reaction, and the ZrB_2 particles were successfully introduced into the spray-formed 7055 aluminum alloy welded joints by TIG welding. The microstructure, hardness, and tensile strength of the welded joints were tested by metallographic microscope, SEM, EDS, Vickers hardness tester, and tensile testing machine. The results show that the microstructure of ZrB_2/7055 welded joints is fine dendrites. The hardness of the weld zone of the ZrB_2/7055 welded joint is higher than that of the 7055 welded joint. With the increase of ZrB_2 particles' content, the tensile strength of welded joints increases first and then decreases. When the content of ZrB_2 particles is 1.5 wt.%, the tensile strength reaches the maximum value of 280 MPa. The tensile strength of the welded joint containing 1.5 wt.% ZrB_2 particles is 14% higher than that of the pure 7055 aluminum alloy welded joint.

1. Introduction

Aluminum alloy is one of the most widely used lightweight materials in industry, and its usage is only inferior to that of steel. It has high strength, good plasticity, excellent conductivity, thermal conductivity, and corrosion resistance. 7XXX series aluminum alloy is called the high-strength aluminum alloy, while the 7055 aluminum alloy is called the super high-strength aluminum alloy, which is widely used in aerospace, rail transit, shipbuilding, and other fields [1–4]. The properties of the spray-formed 7055 high strength aluminum alloy are obviously better than those of the cast aluminum alloy because of its fine grain size, uniform structure, small segregation, and high density. Mg and Zn elements are easy to burn during the fusion welding process, which leads to uneven chemical composition of the weld metal of the spray-formed 7055 aluminum alloy, reduces precipitation of strengthening phases, and makes the strength of the welded joint low [5]. In addition, the welding zone will experience a higher thermal cycle during welding, which also leads to the softening of the welded joint [6, 7].

Many studies show that friction stir welding has the advantages of small heat input, small weld grain, no need to add welding wire, and small residual stress and deformation after welding. Therefore, friction stir welding is the main method used to weld the 7XXX series aluminum alloy [8–12]. However, the friction stir welding process is fully mechanized, and the workpiece needs to be constrained in well-designed fixtures; as a result, it is difficult to weld complex components. Therefore, the special complex components still have to be connected by fusion welding.

The aluminum alloy welding wire is the necessary filling material for fusion welding, which is one of the important factors to determine the welding quality [13]. The commonly used welding wire of the aluminum alloy is the Al-Mg welding wire [14]. Under the correct welding process parameters, although traditional aluminum alloy welding wires can overcome the defects of welding cracks and pores, it is difficult to solve the key welding problem of low strength of the welded joint [14]. Ceramic particle-reinforced aluminum matrix composites have excellent properties such as high specific strength, good wear resistance, high hardness, and

good thermal stability, which integrate the advantages of the matrix and reinforcement phase. Many studies show that 7-series aluminum matrix composites with hard ceramic particles have excellent mechanical properties [15–17]. Many studies have shown that the mechanical properties of welded joints can be improved by using the welding wire containing ceramic particles in the argon arc welding process [18–24]. At present, there are few reports about the effect of welding wires containing ZrB_2 particles on microstructure and mechanical properties of the spray-formed 7055 aluminum alloy TIG welded joint.

In this paper, ZrB_2/Al-Mg and ZrB_2/7055 welding wires were prepared by the in situ reaction method. The effects of ZrB_2 particles on microstructure, hardness, and mechanical properties of spray-formed 7055 aluminum alloy TIG welded joints were studied. The base metal was used as welding wire for the comparative test (corresponding to the pure 7055 welded joint).

2. Experiment Methods

1.5 wt.% ZrB_2/Al-Mg, 1.5 wt.% ZrB_2/7055, and 3.0 wt.% ZrB_2/7055 welding wires were prepared by the in situ reaction method. The matrix for the experiment are pure aluminum (purity > 99%), pure magnesium (purity > 99%), pure copper (purity > 99%), and pure zinc (purity > 99%). The salt used in in situ reaction are K_2ZrF_6 powder (purity > 98%) and KBF_4 powder (purity > 98%). After mixing K_2ZrF_6 and KBF_4 salt powders uniformly, dry them at 250°C for 2 hours.

When the pure aluminum was heated to 850°C in the graphite crucible of the resistance furnace and completely melted, the prepared salt was added into the melt and ZrB_2 particles were generated by the in situ reaction. During the process of reaction, the electromagnetic agitator was turned on, and the time for the reaction was 20 min. When the temperature dropped to 750°C, pure copper and pure zinc were added in proportion of the 7055 aluminum alloy, and the time for the reaction was 10 min. The pure magnesium was added when the temperature dropped to 720°C. After the magnesium was melted completely, the melting liquid was poured into the copper mold. Subsequently, cast was acquired. Wire cutting is then adopted for the aluminum ingot to obtain the welding wire. The specific processes are as follows: firstly, the parts with casting defects on four sides of the aluminum ingot are removed. Secondly, the remaining aluminum ingots were cut into aluminum wires with a cross section of $4 \times 4\,mm^2$. Finally, after cleaning the aluminum wires before welding, they are connected to the required length by spot welding. The aluminum ingots, welding wires before spot welding, and welding wires after spot welding are shown in Figure 1. As shown in Table 1, the main elements (tested by the direct reading spectrometer) of the welding wire are given.

The MAGIC WAVE 2600 TIG welder was used in this experiment. The weld parameters are shown in Table 2. The extruded spray-formed 7055 aluminum alloy (length 300 mm, width 150 mm, and thickness 5 mm) was chosen to weld with a V-shaped groove (60°) in the center. The blunted edge is 2 mm, and the gap is 3–5 mm. The form of the weld joint is butt. Before welding, the oil and the oxide film on the surface of the welding wire and base metal (BM) should be treated, and the cleaned weld wire and BM should be welded within 8 hours. After the weld is completed, the weld roots located in the back sides need to be removed. Figure 2 shows the weld bead morphology after welding with different welding wires.

The element content of the welding wire was detected by the direct reading spectrometer. Taking the center line of the weld as the axis of symmetry, the metallographic samples (length 40 mm, width 4 mm, and thickness 5 mm) were cut by wire cutting. Keller's reagent was chosen as the etchant, and the time for etching is 12 s. The metallography was analyzed by the Axioskop2-MAT optical microscope (OM), and the microstructure of the weld and the fracture morphology of the tensile sample were examined by the Merlin Compac field emission scanning electron microscope (FESEM). Hardness was measured by the MVS-1000QZD Vickers hardness tester at the loading force of 100 g, and the loading time is 10 s. Tensile strength was measured by the CMT5205 electron universal testing machine at the speed of 12 mm/min. The tensile sample was designed according to GB-T2651-2008. The performance of the weld joint for each condition was the average value of three samples.

3. Experimental Results and Discussion

3.1. Microstructure of Welded Joints. Figure 3 shows the photos of welded joints. Figures 3(a) and 3(b) show that there are no cracks at the fusion line of the pure 7055 welded joint and 1.5 wt.% ZrB_2/7055 welded joint, indicating that the weld metal has good bonding with the base metal. Figures 3(c) and 3(d) show that there are obvious cracks at the fusion lines on both sides of 1.5 wt.% ZrB_2/Al-Mg welded joint, which indicates that the bonding between 1.5 wt.% ZrB_2/Al-Mg weld metal and base metal is poor.

The SEM surface morphology and elemental surface scanning of the crack of 1.5 wt.% ZrB_2/Al-Mg welded joint are shown in Figure 4. Figure 4(a) shows that 1.5 wt.% ZrB_2/Al-Mg welded joint is the intergranular cracking, and there are some inclusions at the crack of the welded joint. Figure 4(b) shows that Cu elements are mainly distributed on the grain boundary. Al, Mg, and Zn elements are uniformly distributed on the matrix. The inclusions in the crack contain more oxygen; it can be inferred that the inclusions are oxides. It can be seen from Figures 4(a) and 4(b) that the precipitates on the grain boundary contain Cu, Zn, and Mg elements, but the precipitates are not compact and have poor bonding with the matrix. This is because the composition of the 1.5 wt.% ZrB_2/Al-Mg welding wire is different from that of the base metal, and the expansion coefficient is also different. Therefore, under the action of solidification shrinkage force, the dense precipitates with good bonding with the matrix cannot be formed, and the fusion line cracks. In addition, the inclusion at the fusion line will produce stress concentration and become the crack source. Therefore, the welding wires with the same or similar composition

Figure 1: Preparation of welding wires. (a) The aluminum ingots. (b) Welding wires before spot welding. (c) Welding wires after spot welding.

Table 1: Main elements' composition of the welding wires.

	Zn (wt.%)	Mg (wt.%)	Cu (wt.%)	ZrB_2 (wt.%)	Al (wt.%)
1.5% ZrB_2/Al-Mg	—	5.399	—	1.5	Allowance
1.5% ZrB_2/7055	9.003	2.312	2.366	1.5	Allowance
3.0% ZrB_2/7055	8.988	2.215	2.224	3.0	Allowance

Table 2: Welding parameters.

Current (A)	Speed ($mm \cdot min^{-1}$)	Argon flow rate ($L \cdot min^{-1}$)	Nozzle diameter (mm)
160	100	20	8

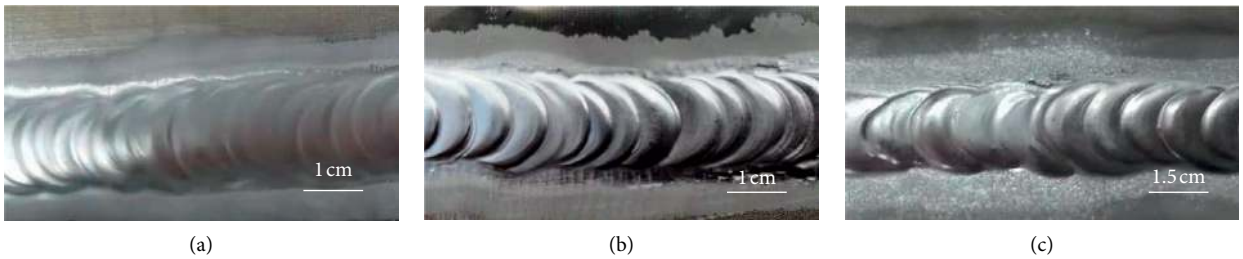

Figure 2: Weld bead morphology after welding with different welding wires. (a) Pure 7055 weld bead. (b) 1.5 wt.% ZrB_2/7055 weld bead. (c) 1.5 wt.% ZrB_2/Al-Mg weld bead.

to the base metal can avoid cracking in the fusion zone of the welded joint and obtain a good welded joint.

Figure 5 shows the metallographic structure of ZrB_2/7055 welded joints. Figure 5(a) shows that the microstructure of the pure 7055 welded joint is a coarse structure with grain size of 70–120 μm. Figure 5(b) shows that the 1.5 wt.% ZrB_2/7055 welded joint is cellular dendrites with grain size of 20–70 μm. Figure 5(c) shows that 3.0 wt.% ZrB_2/7055 welded joint is a fine dendrite grain with the size of 20–50 μm. As the ZrB_2 particles' content increases from 0 wt.% to 3.0 wt.%, the size of the grain becomes more and more smaller. Compared with the pure 7055 welded joint, the grain size of ZrB_2/7055 welded joints is obviously refined, which is due to the ZrB_2 particles increasing the nucleation point and hindering the grain growth during the solidification of the weld metal.

Figure 6 shows the XRD patterns of ZrB_2/7055 welded joints, SEM surface morphology, and elemental surface scanning of ZrB_2/7055 welded joints. It can be seen from Figure 6(a) that the pure 7055 welded joint is composed of α-Al, $MgZn_2$, and Al_2Cu phases. The ZrB_2/7055 welded joints are composed of α-Al, ZrB_2, $MgZn_2$, and Al_2Cu phases. With the increasing of ZrB_2 particles' content, the intensity of the ZrB_2 diffraction peak increases gradually. It can be seen from Figures 6(b) and 6(d) that there are Al, Mg, Zn, and Cu elements in the grain boundary and in the grain of pure 7055 weld. According to XRD, the precipitates in the welded joint are $MgZn_2$ phases, while Cu elements are in $MgZn_2$ phases in the form of the solid solution. The shape of precipitates is regular. It can be seen from Figures 6(c) and 6(e) that the irregular flocculents in the 1.5 wt.% ZrB_2/7055 welded joint contain a large amount of Zr elements, so it can be inferred that the irregular flocculents are ZrB_2 particles. $MgZn_2$ phases with regular shape also precipitate in the 1.5 wt.% ZrB_2/7055 welded joint.

Figure 7 shows the SEM surface morphology of ZrB_2/7055 welded joints. Figures 7(a)–7(c) show that, with the increase of ZrB_2 particles' content, the flocculent ZrB_2 particles in ZrB_2/7055 welded joints gradually increase. Figure 7(d) shows that the flocculent ZrB_2 particles in the

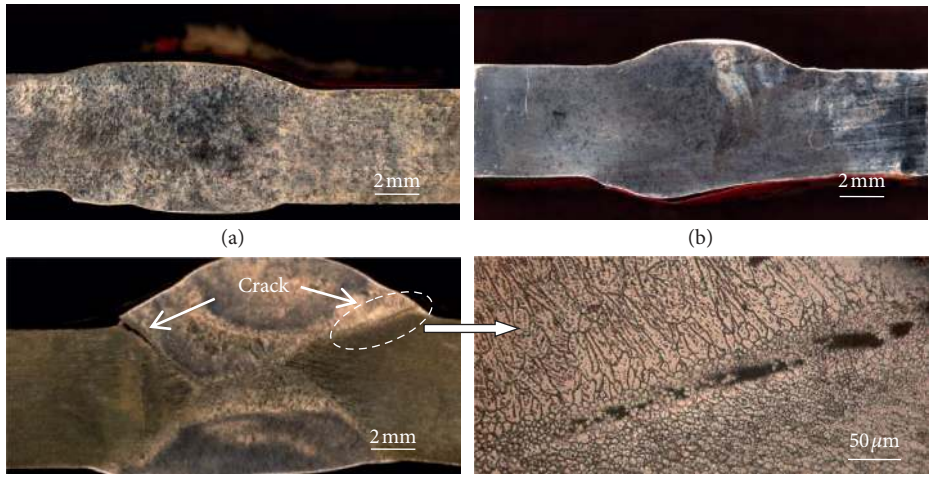

Figure 3: Photos of welded joints. (a) Pure 7055 welded joint. (b) 1.5 wt.% ZrB_2/7055 welded joint. (c) and (d) 1.5 wt.% ZrB_2/Al-Mg welded joint.

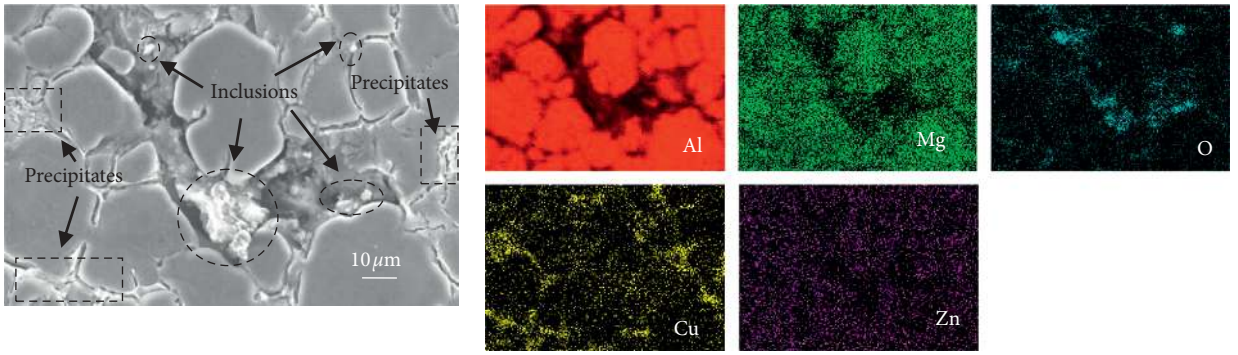

Figure 4: The SEM surface morphology and elemental surface scanning of the crack of 1.5 wt.% ZrB_2/Al-Mg welded joint. (a) SEM surface morphology. (b) Elemental surface scanning of the Al, Mg, O, Cu, and Zn elements.

Figure 5: Metallographic structure of ZrB_2/7055 welded joints with different contents of ZrB_2 particles. (a) Pure 7055 welded joint. (b) 1.5 wt.% ZrB_2/7055 welded joint. (c) 3.0 wt.% ZrB_2/7055 welded joint.

welded joint are composed of many single ZrB_2 particles with the size of hundreds of nanometers. In the process of TIG welding, when ZrB_2 particles enter the molten pool with welding wires, there are two behaviors as follows: on the one hand, in this experiment, the temperature of the molten pool is about 750°C. ZrB_2 and Al liquids are not well wetted at this temperature. During the solidification of the ZrB_2-7055 welded joint, the ZrB_2 particles entering the molten pool are repelled by the solidification interface. In order to reduce the surface energy, they tend to agglomerate. On the other hand, the flocculent ZrB_2 particles disperse and gather under the influence of arc impact and molten pool boiling. However,

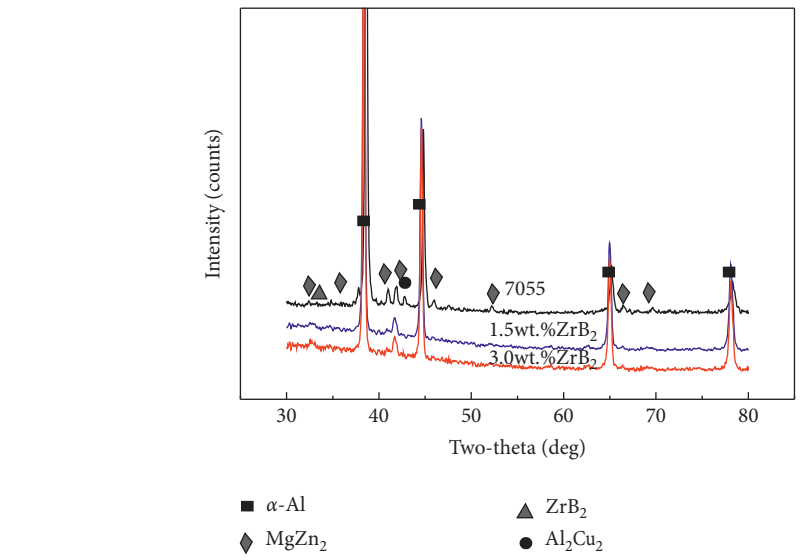

(a)

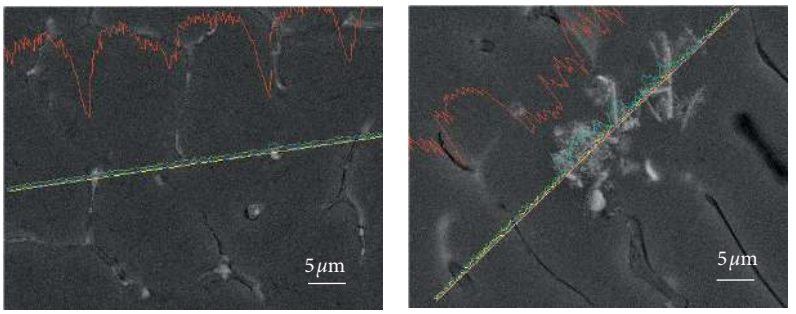

(b) (c)

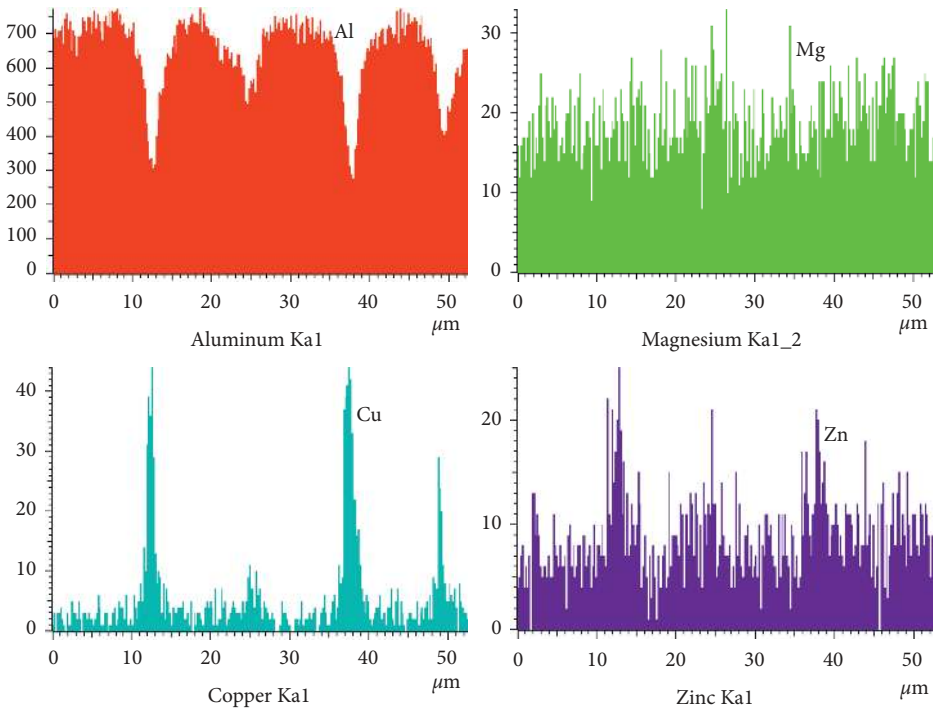

(d)

Figure 6: Continued.

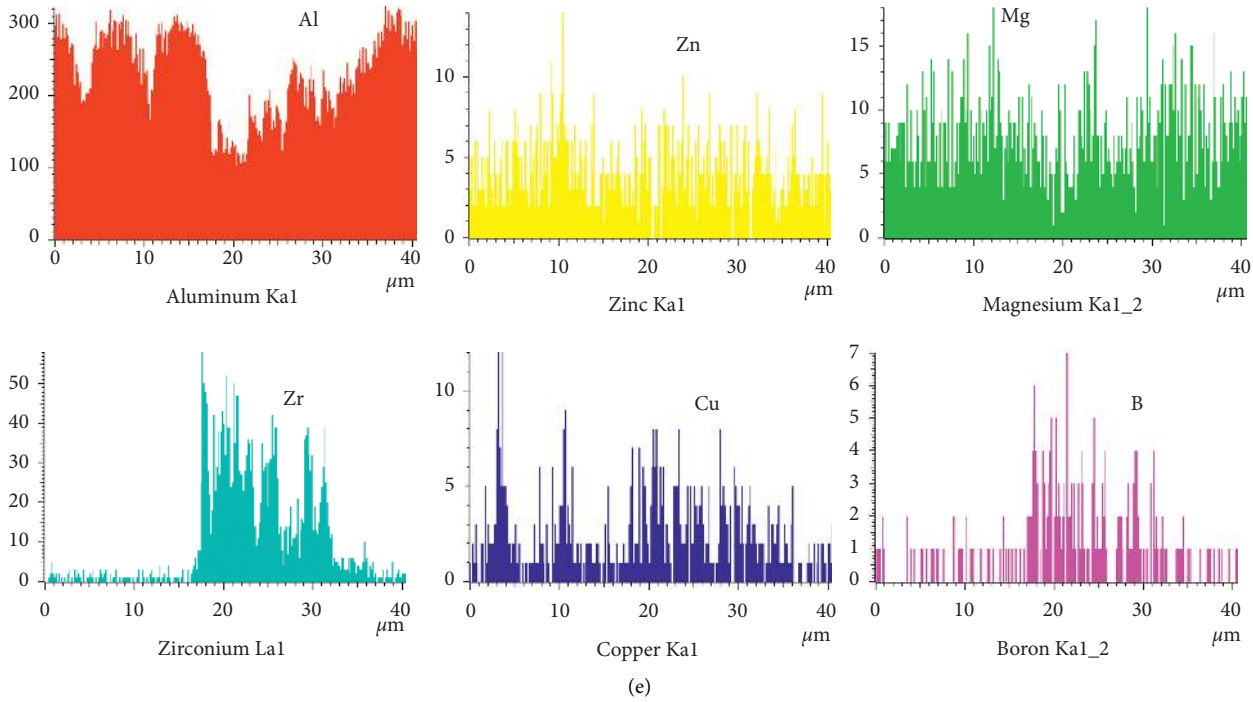

Figure 6: XRD patterns of ZrB_2/7055 welded joints, SEM surface morphology, and elemental surface scanning of ZrB_2/7055 welded joints. (a) XRD patterns. (b) SEM surface morphology of the 7055 welded joint. (c) SEM surface morphology of 1.5 wt.% ZrB_2/7055 welded joint. (d) Elemental surface scanning of the 7055 welded joint. (e) Elemental surface scanning of 1.5 wt.% ZrB_2/7055 welded joint.

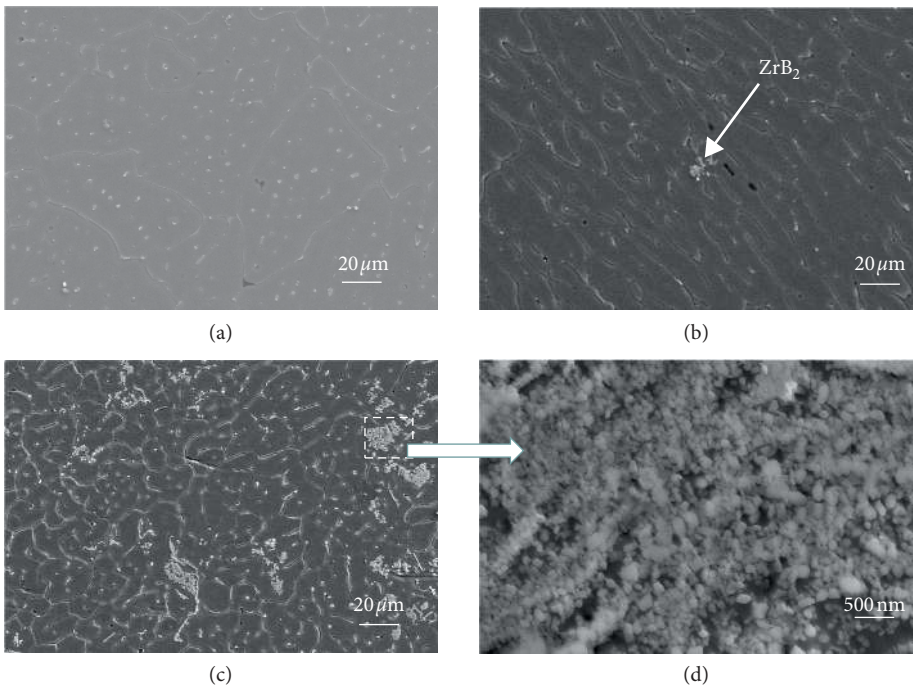

Figure 7: SEM surface morphology of ZrB_2/7055 welded joints. (a) Pure 7055 welded joint. (b) 1.5 wt.% ZrB_2/7055 welded joint. (c) and (d) 3.0 wt.% ZrB_2/7055 welded joint.

the thermal conductivity of the aluminum alloy is large, and the volume of molten pool is small. When the welding heat source leaves the welding position, the molten pool metal solidifies rapidly. The flocculent ZrB_2 particles do not have enough time to disperse completely. Therefore, ZrB_2 particles exist in the welded joints in the form of agglomeration. ZrB_2 particles have the following effects on the solidification behavior of the welded joint. First, ZrB_2 particles can be used

as an effective substrate for -Al phase nucleation during solidification to promote heterogeneous nucleation. Second, the existence of ZrB_2 particles reduces the dendrite growth rate at the liquid-solid interface, increases the undercooling degree near the liquid-solid interface, further promotes the heterogeneous nucleation, and refines the grains.

3.2. Mechanical Properties

3.2.1. Hardness of Welded Joints. Figure 8 shows the hardness of 7055 and 1.5 wt.% ZrB_2/7055 welded joints. It can be seen from Figure 8 that the hardness of the weld zone of the 1.5 wt.% ZrB_2/7055 welded joint is higher than that of the 7055 welded joint. The hardness of the heat affected zone of 7055 and 1.5 wt.% ZrB_2/7055 welded joints are similar. The hardness of the base metal is about 95 HV because the base metal is extrusion 7055 aluminum alloy (without heat treatment). According to Figure 7, the grain size of the 1.5 wt.% ZrB_2/7055 weld zone is smaller than that of the 7055 weld zone, so the enhancement of hardness of the 1.5 wt.% ZrB_2/7055 weld zone is mainly due to grain refinement. Jiang et al. [25] and Patel et al. [26] analyzed the reasons for the increase of hardness of aluminum alloy welded joints, and the results showed that the grain refinement can improve the hardness of the welded joint. In addition, the ZrB_2 particles in the weld zone also contribute to the increase of hardness.

3.2.2. Tensile Properties of Welded Joints. Table 3 shows the values of tensile strength of ZrB_2/7055 welded joints with different contents of ZrB_2 particles. Table 3 shows that, with the increase of ZrB_2 particles' content, the tensile strength of ZrB_2-7055 welded joints first increases and then decreases. When the content of ZrB_2 particles is 1.5 wt.%, the tensile strength of the ZrB_2/7055 welded joint reaches the maximum value of 280 MPa. When the content of ZrB_2 particles is 3.0 wt.%, the tensile strength of the ZrB_2/7055 welded joint decreases to 260 MPa. It can be seen that the tensile strength of the spray-formed 7055 TIG welded joints can be improved by introducing ZrB_2 particles. Figure 9 shows the SEM morphology of the fracture surface of ZrB_2/7055 welded joints with different contents of ZrB_2 particles. Figure 9(a) shows that the pure 7055 welded joint is a typical brittle fracture. Figures 9(b) and 9(c) show that the 1.5 wt.% ZrB_2/7055 and 3.0 wt.% ZrB_2/7055 welded joints are also brittle fracture.

Combined with the microstructure of the welded joints, $MgZn_2$ strengthening phases are found in all three kinds of welds, and $MgZn_2$ phases containing Cu elements also play a role in solution strengthening. Compared with the welded joints with ZrB_2 particles, the pure 7055 welded joint is coarse dendrite, so its tensile strength is the lowest, and it is brittle fracture. For the welded joints containing ZrB_2 particles, there are two main reasons for the improvement of the tensile strength. First, the ZrB_2 particles in the welded joints can act as the second phase pinning dislocation during tensile deformation and play the second phase strengthening role. Second, ZrB_2 particles can refine the grain size of

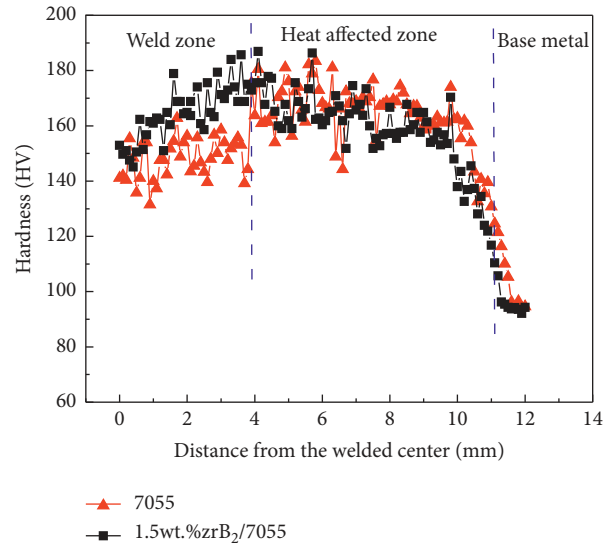

Figure 8: Hardness of 7055 and 1.5 wt.% ZrB_2/7055 welded joints.

Table 3: Tensile strength of ZrB_2/7055 welded joints with different contents of ZrB_2 particles.

	7055	1.5 wt.% ZrB_2/7055	3.0 wt.% ZrB_2/7055
Tensile strength (MPa)	245	280	260

welded joints and play the role of fine grain strengthening. The results of the literature [27] also show that the grain refinement is the important reason for the tensile strength improvement of the Al-Zn-Mg-Cu alloy. Based on the above two points, it can be inferred that the tensile strength of the welded joint with 3.0 wt.% ZrB_2 particles should be the maximum. However, it can be seen from Table 3 that the tensile strength of the 1.5 wt.% ZrB_2/7055 welded joint is higher than that of the 3.0 wt.% ZrB_2/7055 welded joint. This is because there are more flocculent ZrB_2 particles in the 3.0 wt.% ZrB_2/7055 welded joint than those in the 1.5 wt.% ZrB_2/7055 welded joint. A large number of flocculent particles will decrease the toughness of the aluminum matrix. The combination of flocculent particles and matrix will be gradually destroyed during the tensile process, resulting in cracks and the reduction of tensile strength.

From the studies of particle-reinforced metal matrix composites, we found that the distribution of particles has a great influence on the microstructure and properties of the materials. Ceramic particles with good wettability can be evenly distributed on the matrix, and the matrix structure changes from dendrite to fine equiaxed crystal. Fine equiaxed crystal can improve the strength and plasticity of the matrix at the same time. But, in this experiment, the distribution of ZrB_2 particles in the welded joints is nonuniform, which is due to the bad wettability between ZrB_2 and liquid Al. Therefore, in order to prepare the welded joint with uniform dispersion of ceramic particles, it is necessary to select the particles with good wettability with the base metal of the molten pool. We think that the spray-formed 7055 aluminum alloy welded joint with high strength and

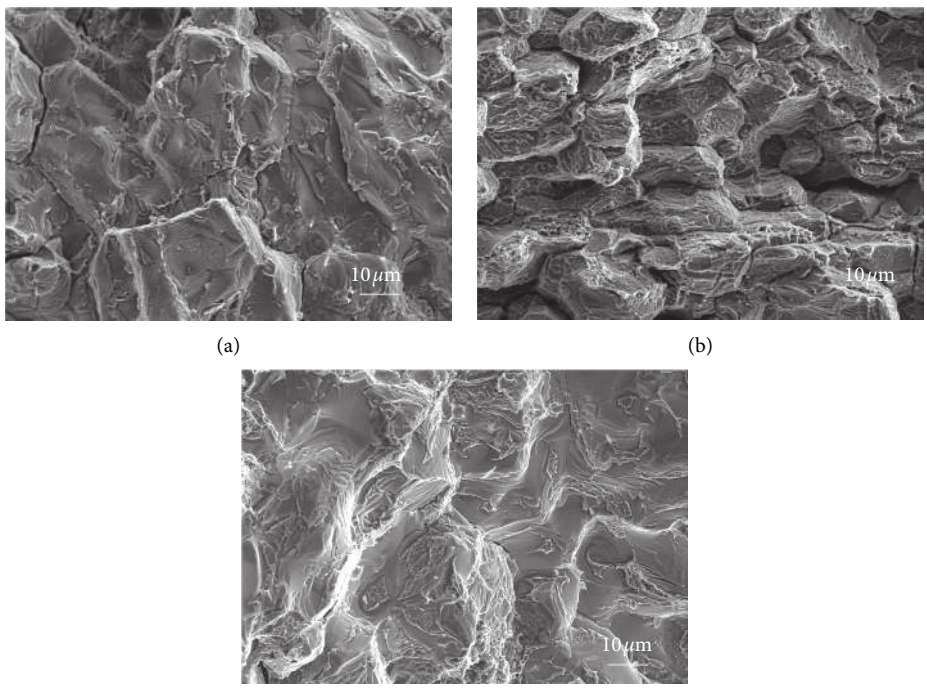

(a) (b) (c)

Figure 9: SEM morphology of the fracture surface of ZrB_2/7055 welded joints. (a) Pure 7055 welded joint. (b) 1.5 wt.% ZrB_2/7055 welded joint. (c) 3.0 wt.% ZrB_2/7055 welded joint.

plasticity can be obtained by adding ceramic particles with good wettability to the matrix.

4. Conclusion

In this paper, a series of welding wires containing ZrB_2 particles were developed and used for TIG welding of the spray-formed 7055 aluminum alloy. This study provides a theoretical basis for further expanding the application of the spray-formed 7055 aluminum alloy. The results are as follows.

(1) With the increase of ZrB_2 particles' content, the grain size of ZrB_2/7055 welded joints decreases gradually. ZrB_2 particles are mainly flocculent in the weld and distributed in the grain boundary and in the grain.

(2) With the increase of ZrB_2 particles' content, the tensile strength of ZrB_2/7055 welded joints first increases and then decreases. The tensile strength of 1.5 wt.% ZrB_2/7055 welded joint is the highest, which is 280 MPa. The tensile strength of the pure 7055 welded joint is only 245 MPa. Compared with the pure 7055 welded joint, the tensile strength of the 1.5 wt.% ZrB_2/7055 welded joint is increased by about 14%.

Data Availability

No data were used to support the findings of this study.

Conflicts of Interest

The authors declare that they have no conflicts of interest.

Acknowledgments

This work was supported by Graduate Research and Innovation Projects of Jiangsu Province (CN) (KYCX20_3098).

References

[1] Y. Yang, Y. Zhao, X. Kai et al., "Effects of hot extrusion and heat treatment on microstructure and properties of industrial large-scale spray-deposited 7055 aluminum alloy," *Materials Research Express*, vol. 5, no. 1, Article ID 016519, 2018.

[2] Y. W. Liu, R. J. Zhang, J. H. Liu, L. Li, H. Y Wang, and G. R. Peng, "Influence of NaCl on dechromization of Cu-Cr-Al alloy in H_3PO_4 solution," *Transactions of Nonferrous Metals Society of China*, vol. 20, no. 1, pp. 123–127, 2010.

[3] T. S. Srivatsan, S. Anand, and S. Sriram, "The high-cycle fatigue and fracture behavior of aluminum alloy 7055," *Materials Science and Engineering: A*, vol. 281, no. 1-2, p. 292, 2000.

[4] H. Yu, M. Wang, X. Sheng et al., "Microstructure and tensile properties of large-size 7055 aluminum billets fabricated by spray forming rapid solidification technology," *Journal of Alloys and Compounds*, vol. 578, p. 208, 2013.

[5] P. Wang, "Corrosion resistance and high temperature wear," *Lanzhou University of Technology*, vol. 43, 2016.

[6] S. C. Wu, T. Tang, and L. I. Zheng, "Modern welding technology," *Robotic Welding Technology*, vol. 32, no. 2, p. 5, 2011.

[7] S. Wan and J. S. Yao, *The Welding of Aluminum and Aluminum Alloys*, China Machine Press, Beijing, China, 2006.

[8] Q. Wang, Y. Zhao, and K. Yan, "Corrosion behavior of spray formed 7055 aluminum alloy joint welded by underwater friction stir welding," *Materials & Design*, vol. 68, pp. 97–103, 2015.

[9] L. L. Liu, Q. L. Pan, X. D. Wang, and S. W. Xiong, "The effects of aging treatments on mechanical property and corrosion behavior of spray formed 7055 aluminium alloy," *Journal of Alloys and Compounds*, vol. 735, pp. 261–273, 2018.

[10] Q. Wang, Z. Zhao, Y. Zhao, K. Yan, and H. Zhang, "The adjustment strategy of welding parameters for spray formed 7055 aluminum alloy underwater friction stir welding joint," *Materials & Design*, vol. 88, pp. 1366–1376, 2015.

[11] T. Sun, M. J. Roy, D. Strong, and C. Simpson, "Weld zone and residual stress development in AA7050 stationary shoulder friction stir T-joint weld," *Journal of Materials Processing Technology*, vol. 263, 2018.

[12] V. Patel, W. Li, G. Wang, F. Wang, P. Niu, and P. Vairis, "Friction stir welding of dissimilar aluminum alloy combinations: state-of-the-art," *Metals-Open Access Metallurgy Journal*, vol. 9, no. 3, 2019.

[13] Y. Li, W. Zou, B. Lee, A. Babkin, and Y. Chan, "Research progress of aluminum alloy welding technology," *International Journal of Advanced Manufacturing Technology*, vol. 109, no. 156, pp. 1207–1218, 2020.

[14] J. Huang, "Augmenting Java method comments generation with context information based on neural networks," *Nanjing University of Aeronautics and Astronautics*, vol. 11, 2016.

[15] S. Devaganesh, P. K. D. Kumar, N. Venkatesh, and R. Balaji, "Study on the mechanical and tribological performances of hybrid SiC-Al7075 metal matrix composites," *Journal of Materials Research and Technology*, vol. 9, no. 3, pp. 3759–3766, 2020.

[16] A. Yj, B. Swa, and S. C. Da, "An interdisciplinary journal of materials science and solid–state chemistry and physics," *Journal of Alloys and Compounds*, vol. 83, Article ID 153504, 2020.

[17] J. Cheng, Y. Ge, B. Z. Wang et al., "Microstructure and tribocorrosion behavior of Al2O3/Al composite coatings: role of Al_2O_3 addition," *Journal of Thermal Spray Technology*, vol. 29, no. 7, 2020.

[18] M. Fattahi, Y. M. Mohammad, I. N. Sajjad et al., "Energy harvesting vibration sources for microsystems," *Journal of Materials Processing Technology*, vol. 217, 2015.

[19] M. Fattahi, N. Nabhani, E. Rashidkhani et al., "A new technique for the strengthening of aluminum tungsten inert gas weld metals: using carbon nanotube/aluminum composite as a filler metal," *Micron*, vol. 54-55, no. 6, pp. 28–35, 2013.

[20] M. Fattahi, V. N. Aghaei, A. R. Dabiri et al., "Novel manufacturing process of nanoparticle/Al composite filler metals of tungsten inert gas welding by accumulative roll bonding," *Materials Science and Engineering A*, vol. 648, pp. 47–50, 2015.

[21] A. R. Dabiri, R. Y. Mojallal, E. Ahmadi, M. Fattahi, Y. Fattahi, and S. Amirkhanlou, "Effect of ZrO_2 nanoparticles on the impact properties of shielded metal arc welds," *Materials Letters*, vol. 158, pp. 325–328, 2015.

[22] E. Ahmadi, M. Ranjkesh, E. Mansoori, Y. Fattahi, S. Amirkhanlou, and R. Y. Mojallal, "Microstructure and mechanical properties of Al/ZrC/TiC hybrid nanocomposite filler metals of tungsten inert gas welding fabricated by accumulative roll bonding," *Journal of Manufacturing Processes*, vol. 26, p. 173, 2017.

[23] I. A. Sabetghadam, H. Zalaghi, S. Hashempour, M. Fattahi, Y. Fattahi, and S. Amirkhanlou, "Fabrication and properties of ZrO_2/AZ31 nanocomposite fillers of gas tungsten arc welding by accumulative roll bonding," *Archives of Civil & Mechanical Engineering*, vol. 16, no. 3, pp. 397–402, 2016.

[24] M. Sokoluk, C. Cao, S. Pan, and X. Li, "Nanoparticle-enabled phase control for arc welding of unweldable aluminum alloy 7075," *Nature Communications*, vol. 10, no. 1, 2019.

[25] H. J. Jiang, B. Zhang, C. Y Liu et al., "Advance in antibacterial magnesium alloys and surface coatings on magnesium alloys: a review," *Acta Metallurgica Sinica*, vol. 32, no. 9, p. 1135, 2019.

[26] V. Patel, W. Li, A. Vairis et al., "A review on friction stir-based channeling," *Critical Reviews in Solid State and Materials Sciences*, vol. 378, 2019.

[27] C. A. Orozco, L. M. Alvarez, D. Verdera, P. Rey, R. A. Oscar, and C. Ferrando, "Evaluation of the mechanical anisotropy and the deformation mechanism in a multi-pass friction stir processed Al-Zn-Mg-Cu alloy," *Materials and Design*, vol. 125, 2017.